JOURNAL OF THERMOPHYSICS AND HEAT TRANSFER
Vol. 19, No. 3, July–September 2005

Absorption Spectroscopy for Temperature Measurement Behind Shock Wave at Super-Orbital Velocity

Atsushi Matsuda*
University of Tokyo, Tokyo 113-8654, Japan
and
Kazuhisa Fujita,† Shunichi Sato,‡ and Takashi Abe§
Institute of Space and Astronautical Science, Kanagawa 229-8510, Japan

The distribution of the translational temperature of atomic oxygen behind the strong shock wave in air produced in a shock tube was measured by means of an unique absorption spectroscopic technique. The translational temperature was determined by fitting a Voigt profile to the measured absorption spectral line shape. The translational temperature behind a shock wave with an initial pressure of 0.3 torr and a shock propagation velocity of 12 km/s showed a fairly good agreement with a numerical prediction, at least qualitatively, and enables confirmation of the phenomenon of the lower rotational temperature compared to the translational temperature, which was suggested previously. Simultaneously, the distribution of electron density was also determined from the absorption spectral profile and showed a reasonable agreement with the previous experimental result based on the emission spectroscopic technique for a Balmer line of hydrogen. This agreement suggests the validity of the present result.

Nomenclature

B	=	Einstein's B coefficient
c	=	velocity of light
E_p	=	resonance level excitation energy for perturbers
g	=	statistical degeneracy
$\hbar$	=	Planck constant
I_0	=	incident laser intensity
$I(\lambda)$	=	laser intensity at wavelength λ
k	=	absorption coefficient
k_b	=	Boltzmann constant
m_e	=	mass of electron
m_o	=	mass of atomic oxygen
N	=	number density of neutral particles
n_e	=	electron density
T_e	=	electron temperature
T_t	=	translational temperature
$\overline{v_m}$	=	relative velocity between perturber and absorber
λ	=	wavelength
λ_c	=	wavelength at absorption center
$\phi(\lambda)$	=	spectral line shape function

Subscripts

m	=	upper energy state
n	=	lower energy state

Presented as Paper 2003-3784 at the AIAA 36th Thermophysics Conference, Orlando, FL, 23–26 June 2003; received 26 July 2004; revision received 22 October 2004; accepted for publication 22 October 2004.

*Graduate Student, Department of Aeronautics and Astronautics, Hongo 7-3-1, Bunkyoku; currently Researcher, The Institute of Space and Astronautical Science, Yoshinodai 3-1-1, Sagamihara, 229-8510, Japan, JAXA; matsuda@gd.isas.jaxa.jp. Student Member AIAA.

†Research Associate; currently Associate Senior Researcher, The Institute of Space Technology and Aeronautics, Chotu, Tokyo, 182-8522, Japan, Yoshinodai 3-1-1, Sagamihara. Member AIAA.

‡Technical Staff, Research Division for Space Transportation, Yoshinodai 3-1-1, Sagamihara.

§Professor, Research Division for Space Transportation, Yoshinodai 3-1-1, Sagamihara. Associate Fellow AIAA.

I. Introduction

A SAMPLE return mission from an asteroid, MUSES-C (Ref. 1), that was developed at the Institute of Space and Astronautical Science in Japan, the spacecraft of which was successfully launched in May 2003, has reactivated research on nonequilibrium flows behind strong shock waves. [2] This is because, in this mission, the return capsule is to reenter into the Earth's atmosphere with an extremely high reentry speed of about 12 km/s. Because of this extremely high reentry speed, the aerothermal heat load to the reentry capsule was expected to be very severe, and, therefore, its quantitative prediction was crucial in the development of the return capsule.

For the prediction of the aerothermal heat load for such a vehicle, one must know the structure of such a strong shock wave. To investigate it, shock-tube experiments have been carried out.[3,4] Hitherto, rotational and vibrational temperatures of N_2 and N_2^+ and electron number density behind strong shock waves have been investigated by means of the emission spectroscopic technique, first for pure nitrogen[3,4] and then for air.[5,6]

These previous investigations have revealed an unpredicted nonequilibrium behavior among the rotational, vibrational, and translational temperatures. In particular, the previous experiment revealed that the rotational temperature is quite low behind the shock front[3,6] compared with the translational temperature, which, however, was not directly measured, but was only anticipated based on the theoretical model. Therefore, measuring experimentally the translational temperature enables us to confirm the expectation of the nonequilibrium among the translational and rotational temperatures. For this purpose, we attempt to measure the translational temperature directly.

For this attempt, the laser absorption spectroscopic technique was applied. This is because we can make use of an absorption line of atomic oxygen in highly heated air in which atomic oxygen is generated through a dissociation process. For this absorption, was selected the absorption line of the atomic oxygen or OI($3p^5P \rightarrow 3s^5S$) (Ref. 7) transition at a wavelength of 777.194 nm. The energy diagram of atomic oxygen is shown in Fig. 1 (Ref. 8). As shown in Fig. 1, the lower state for this transition ($3s\ ^5S$) is a metastable state, that is, there is no optically allowed transition between this state and the states below it. Because the lifetime of the atom in the metastable state is relatively long, the number density of the state tends to be large, and, therefore, the absorption intensity tends to be strong.

By measurement of the absorption spectral line profile, it is possible, in general, to determine the translational temperature and the

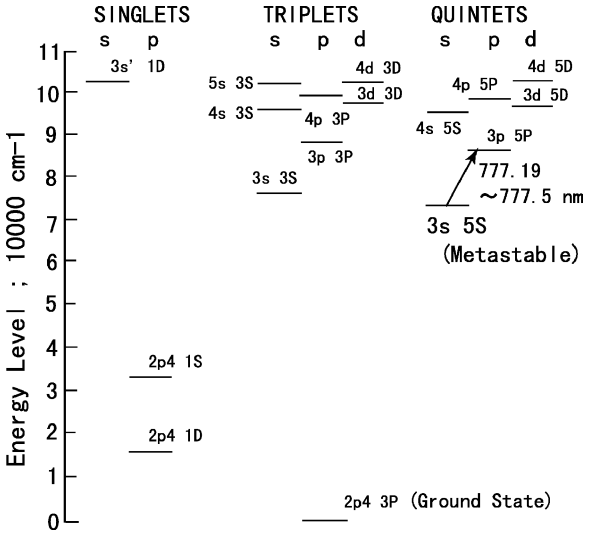

Fig. 1 Energy diagram of atomic oxygen.[8]

number density of the atomic oxygen in the lower state of the absorption line. In the case that the absorption profile is broadened by the Stark effect, it may also be possible to determine the electron number density as well. Nevertheless, it may be, in general, difficult to apply the standard absorption spectroscopic method to a shock-tube experiment because scanning a spectrum requires a sufficient measuring time that a shock-tube experiment cannot provide. To overcome this difficulty, we have developed a new experimental technique in this paper.

II. Theoretical Background

The laser beam intensity passing through a uniform plasma with the absorption coefficient can be written as

$$I(\lambda)/I_0 = \exp[-k(\lambda)x] \tag{1}$$

The absorption coefficient $k(\lambda)$ for the wavelength λ is defined as

$$k(\lambda) = (h/\lambda_c)B_{mn}N_m\,[1 - (N_n/N_m)(g_m/g_n)]\,\phi(\lambda) \tag{2}$$

where the line shape function $\phi(\lambda)$ reflects the thermochemical properties of the plasma under consideration and, thus, is influenced by various effects such as the thermal motion of the particles and collisions among them. For the line shape function, the Gaussian, Lorentzian, and Voigt profiles are known, theoretically, to appear depending on those effects.

In the following subsections, we briefly estimate the order of magnitude of those effects expected in the present shock-tube experiment, assuming a shock wave that propagates in air of 0.3 torr with a speed of 12 km/s. For this purpose, we consider the equilibrium state behind the shock wave, where translational temperature T_t, electron density n_e, and number density of neutral particles N are approximately 10^4 K, 10^{16} cm^{-3}, and 10^{23} m^{-3}, respectively. Hereafter, we call this a standard state.

A. Doppler Broadening

When the Maxwellian velocity distribution of the absorbing particles (in this case, atomic oxygen) is assumed in the plasma, the half-width of the half-maximum of the Gaussian profile $\Delta\lambda_G$ becomes[9]

$$\Delta\lambda_G = (\ell n 2)^{\frac{1}{2}}(\lambda_c/c)\sqrt{(2k_bT_t/m_O)} \tag{3}$$

In the standard state, $\Delta\lambda_G$ for the OI at $\lambda_c = 777.194$ nm becomes approximately 7×10^{-3} nm.

B. Collisional Broadening

The collisional broadening is mainly caused by the following two types of collisions experienced by the absorbing particle: 1) the collision with charged particles (Stark broadening) and 2) collision with neutral particles (van der Waals broadening).

Table 1 Values of w' and α' for OI at 777.1942 nm at $n_e = 10^{16}$ cm^{-3} and $T_e = 10^4$ K (Ref. 10)

Parameter	Value
Electron impact w', Å	3.27×10^{-2}
Ion broadening α', Å	2.8×10^{-2}

1. Stark Broadening

For a nonhydrogen absorber like atomic oxygen, the half-width of the half-maximum of Stark broadening $\Delta\lambda_S$ in meters is given by Ref. 10,

$$\Delta\lambda_S = \left\{1 + 1.75 \times 10^{-4} n_e^{\frac{1}{4}}\alpha'\left(1 - 0.068T_e^{-\frac{1}{2}}n_e^{\frac{1}{6}}\right)\right\} \times 10^{-26} n_e w' \tag{4}$$

In this equation, n_e is the electron density in negative cubic centimeters, and the quantities w' and α' are the electron impact parameter in angstroms and the ion broadening parameter in angstroms, respectively, which are listed in Table 1. Note that, in the standard state, the ion impact effect can be neglected compared with the electron impact effect. Therefore, Eq. (4) can be simplified as

$$\Delta\lambda_S \sim 1 \times 10^{-26} n_e w' \tag{5}$$

In the standard state, the Stark broadening width $\Delta\lambda_S$ given by Eq. (5) becomes of the order of 4×10^{-3} nm.

2. Van der Waals Broadening

The half-width of the half-maximum of the van der Waals broadening can be represented in meters as[11]

$$\Delta\lambda_W = \frac{N}{2}\left(\frac{9\pi\hbar^5\overline{R_\alpha^2}}{16m_e^3E_p^2}\right)^{\frac{2}{5}}\overline{v_m}^{\frac{3}{5}}\frac{\lambda_c^2}{c} \tag{6}$$

where N is in negative cubic meters, E_p is in joules, and $\overline{v_m}$ is in meters per second. In the present case, $E_p \sim 1.52 \times 10^{-18}$ J. For atomic oxygen, $\overline{R_\alpha^2} \sim 44$ (Ref. 11) at the transition of 777.194 nm. In the standard state, the half-width of the half-maximum estimated by Eq. (6) becomes on the order of 8×10^{-5} nm.

As this estimation shows, the van der Waals broadening is sufficiently smaller than Stark broadening in the present case. Therefore, the collisional broadening is expected to be caused mainly by the Stark effect.

C. Voigt Profile

As discussed earlier, the Stark effect, in the present case, appears to be on the same order as the Doppler effect. Therefore, the line shape function should be approximated by the Voigt profile, which is a convolution of the Gaussian and the Lorentzian profile,

$$H(a, v) = \frac{a}{\pi}\int_{-\infty}^{\infty}\frac{\exp(-y^2)}{a^2 + (v - y)^2}\mathrm{d}y \tag{7}$$

where

$$v = (\ell n 2)^{\frac{1}{2}}(\lambda - \lambda_c)\big/\Delta\lambda_G \tag{8}$$

and the parameter a is the Voigt parameter defined as a ratio between the half-width of the half-maximum of the Gaussian profile ($\Delta\lambda_G$) and that of the Lorentzian profile ($\Delta\lambda_L$),

$$a = \Delta\lambda_L/\Delta\lambda_G \tag{9}$$

The half-width of the half-maximum of the Lorentzian profile ($\Delta\lambda_L$) can be defined as

$$\Delta\lambda_L = \Delta\lambda_S + \Delta\lambda_W \tag{10}$$

which can be approximated as

$$\Delta\lambda_L \sim \Delta\lambda_S \tag{11}$$

in the shock heated region in the present condition.

There are many ways to describe approximately the Voigt profile in Eq. (7), for example, a polynomial approximate function or a tabulated database. In Table 1 given in Ref. 12, for instance, the value of $H(a, v)/H(a, 0)$ for various v with the parameter a from 0 to 10 is tabulated.

Once the experimentally measured absorption profile is available, we can deduce the physical quantities such as the translational temperature T_t and electron density n_e by fitting a Voigt profile to the measured absorption spectrum.

III. Experimental Method

The experiment was conducted by means of the double diaphragm free piston shock tube at the Institute of Space and Astronautical Science (ISAS) in Japan. The shock tube has a cross section of 35×35 mm and can generate shock waves with the propagation velocity up to 13 km/s for the initial pressure of 0.3 torr (Ref. 13). The experimental setup around the measurement section for the absorption spectroscopic technique is shown in Fig. 2. In Fig. 2, the diode lasers A and B, which are tunable diode lasers, Model 6312 Velocity Laser (New Focus, Inc.), are the light sources for the absorption spectroscopy. The spectral linewidth of these lasers are at most 6×10^{-7} nm (300 kHz), which is sufficiently narrower than the expected linewidth and, therefore, ensures a sufficient wavelength resolution for this absorption spectroscopy.

To get the absorption spectrum in the standard absorption spectroscopy for the almost steady phenomena such as the one conducted in Ref. 11, the oscillation wavelength of the laser is scanned continuously over the absorption spectral linewidth. For the shock-tube experiment, however, it is almost impossible to scan the laser wavelength over the linewidth because the scanning speed of the diode laser is much slower than the transient phenomena associated with the shock wave propagation. Fortunately, according to previous experience,[3–6] the present shock tube has a reasonably good reproducibility of the operating condition. Therefore, in the present experiment, there is a possibility to obtain an absorption spectrum by carrying out repeated runs of the shock tube, that is, the transient absorption measurement was undertaken for a fixed laser wavelength in one shock-tube operation, and such an absorption measurement associated with the various laser wavelengths was accumulated by repeated runs of the shock tube. The absorption spectrum at a specific location behind the shock front was compiled from the accumulated data. Even though the reproducibility of the shock tube is fairly good, there still remains a slight deviation in the operating condition from run to run. To compensate for such a slight deviation of the operating condition, two laser beams were made use of, that is, one beam, designated laser B, in Fig. 2 was used for scanning the wavelength, whereas another beam, designated laser A, was used to monitor at the fixed wavelength common for each shock-tube run and was made use of to normalize the measured data for laser B.

As shown in Fig. 2, beam B was set to pass through the center of the measurement section whereas beam A was positioned slightly (10 mm) above it, even though it should be aligned with the path of beam B. For the setup of the beam paths, the plane including these two beams (A and B) was set to be parallel to the shock wave front surface. This slight dislocation in the setup of the beam paths is because of the facility limitation, but may not affect the result because the behavior of the physical quantities such as temperature are expected to be almost uniform in a plane parallel to the shock wave front. The laser wavelength was adjusted before each shock tube run by using the wavelength meter (High Precise Wave Meter, WA-1500-Vis Laser Wave Length Meter, Burleigh EXFO Company), which enables us to adjust the wavelength on the order of 10^{-4} nm. Two laser beams (A and B) were split into two optical paths by means of a cubic beam splitter. One beam path was for monitoring the reference laser beam intensity. Another path was for the measurement. All of the intensities of the four laser beams were monitored independently by the photodetectors labeled from 1 to 4 in Fig. 2. The response time of this photodetector is within 100 nse. These four identical photodetectors were designed to keep the same response time by using a cable of the same length from the detector circuit to the oscilloscope. The narrowband pass filters in front of these four detectors were used to avoid the entrance of the self-radiation generated behind the shock waves.

The arrival of the shock waves to the measurement section was detected by a laser schlieren system composed of an He–Ne laser. In Fig. 2, the system is shown symbolically, simply as an He–Ne laser directed downward. In this paper, the physical quantities behind the shock front will be presented by the distance from the shock front. For this purpose, the passage time from the shock front was converted to the distance from the shock front based on the shock propagation velocity. When all of the effects that should be taken into account are included, the spatial resolution for the physical quantity is within the accuracy of ± 0.6 mm.

IV. Experimental Results

The experiment was carried out for air of an initial pressure of 0.3 torr, in which the shock propagates with a nominal speed of 12.1 km/s.

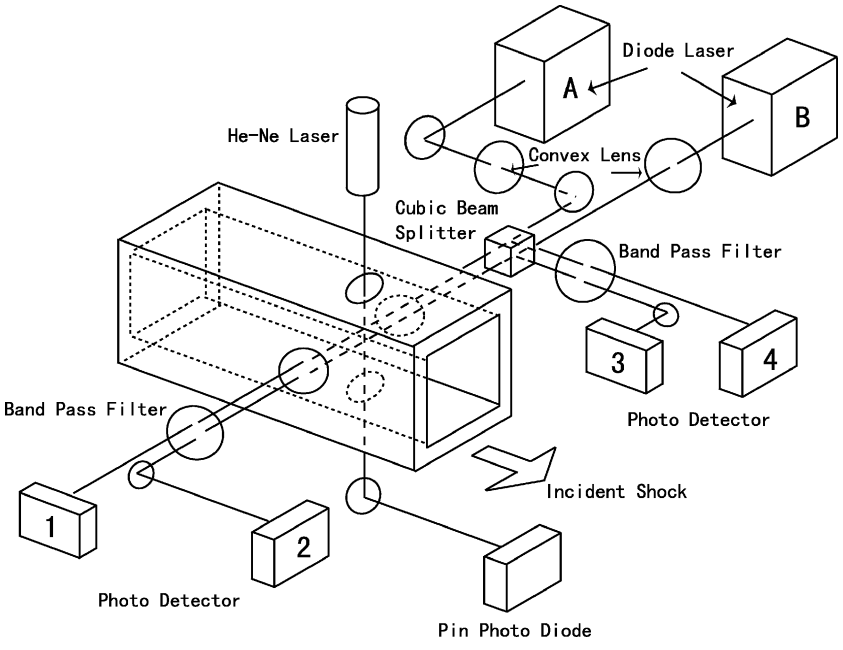

Fig. 2 Experimental setup for absorption spectroscopic technique.

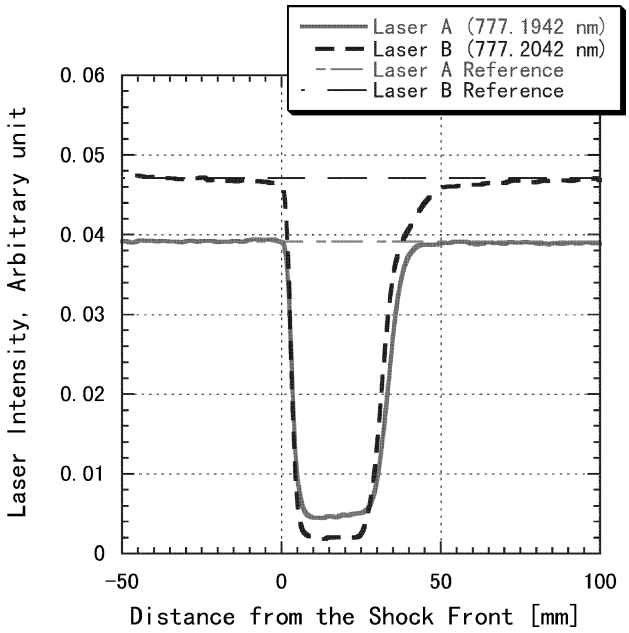

Fig. 3 Laser intensity distribution, $V_s = 12.01$ km/s.

A. Laser Intensity Distribution

The typical laser intensity variations for lasers A and B are shown in Fig. 3. As mentioned in the preceding section, laser A was set at 777.1942 nm and was used as the reference for normalization. Laser B was for scanning the wavelength at the absorption line. The two thin lines show the reference intensities for lasers A and B and were almost constant during the measurement. The horizontal axis represents the distance measured from the shock front. The origin is the shock front detected by the laser schlieren method. The thick lines show the signal for the laser intensity after passing through the measurement section of the shock tube. Before the shock wave arrives at the measurement section, the signal intensity distributions of both lasers are almost steady, whereas they show a rapid decrease just after the shock arrival. This decrease is due to the absorption by the shock-heated air. After the rapid decrease, the laser intensity shows a quite gradual variation at the region between 10 and 20 mm behind the shock wave. After that, the laser intensity rapidly recovers to the intensity observed before the shock wave arrival, at approximately 35 mm behind the shock front.

The absorption of the laser beam is due to the atomic oxygen excited to the $3s^5S$ state, which absorbs the light of the wavelength at 777.194 nm. Such excited atomic oxygen may be produced as a result of the energy exchange process between electrons and atomic oxygen. Therefore, the rapid decrease of the laser intensity observed in Fig. 3 corresponds to the increase of the atomic oxygen in the $3s^5S$ state excited through the energy exchange process. The generation of such atomic oxygen reaches a plateau region as the flow approaches a thermochemical equilibrium state. The gradual variation in the laser intensity following the rapid variation is expected to correspond to the equilibrium state. On the other hand, the successive rapid recovery region may correspond to the contact surface.

B. Absorption Spectrum and Physical Data Determination

The absorption spectrum at the specific location behind the shock wave was obtained by selecting, at the specific location, the data accumulated for various wavelengths in many repeated runs of the shock tube. In each run of the shock tube, the shock propagation speed is kept within 12.1 ± 0.1 km/s.

As mentioned earlier, the absorption spectrum obtained in this experiment is expected to have the Voigt profile, which is a convolution of Gaussian and Lorentzian profiles. To make a fit to the measured spectrum, the database for the Voigt profile was constructed based on Table 1 given in Ref. 12. For the construction of the Voigt profile database, we must specify two parameters, a and T_t, which are the Voigt parameter defined as Eq. (9) and the translational temperature, respectively. For the database, the Voigt parameter a ranges from 0 to 10, whereas the translational temperature T_t ranges from 10^4 to 5×10^4 K at intervals of 1000 K. To make the best fit to the measured data, the residual defined from the measured data and the Voigt profile was minimized. When the best-fitting profile from the database, is found, the translational temperature can be determined. Additionally, when the parameter a is used, the Stark broadening width can be derived, and, therefore, the electron density can be determined by the use of Eq. (5).

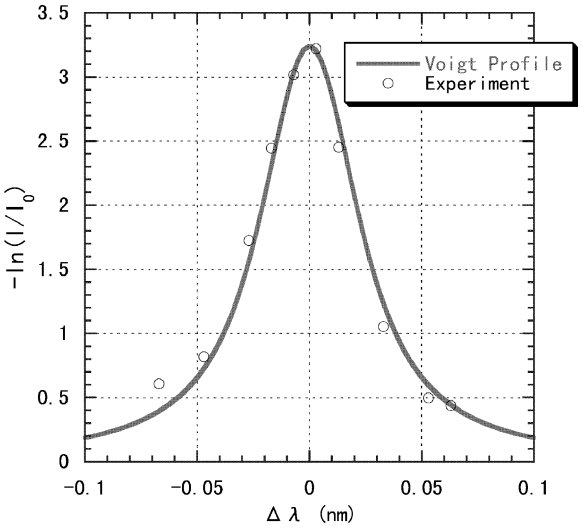

Fig. 4 Absorption profile for shock propagation velocity 12.1 ± 0.1 km/s at 7 mm behind shock front. Voigt parameter $a = 2.6$, $T_t = 1.2 \times 10^4$ K, and $n_e = 7.2 \times 10^{22}$ m^{-3}.

Figure 4 is one of the examples of the Voigt profile fittings that was made at 7 mm behind the shock front. We assume that the absorption strength is uniform along the beam path because the flow properties such as temperature and density in the plane parallel to the shock front are expected to be uniform. Then, the quantity $-\ell_n(I/I_0)$ becomes $k(\lambda)H$, where H is the width of the shock tube, and, thus, is proportional to $k(\lambda)$.

Recall that the boundary-layer growth behind the shock wave may disturb the assumption of the uniformity of the flow in the region. Thus, let us estimate the effect of the boundary layer. In the case of $V_s = 12$ km/s and $L = 10$ mm, the boundary-layer thickness δ becomes at most 0.6 mm. Here, δ at the distance L behind the shock front with the shock propagation velocity V_s was estimated roughly as

$$\delta = L\sqrt{\nu/V_s L} \tag{12}$$

Even for this boundary-layer thickness, the effective cross section of the shock tube is reduced by only 4%, and, therefore, we can conclude that the effect of the boundary-layer growth can be negligible and that the flow can surely be assumed to be almost uniform.

As seen in Fig. 4, the experimental result distributed reasonably around the theoretical profile. From this fitting method, the Voigt parameter a and the translational temperature T_t are determined to be 2.6 and 1.2×10^4 K, respectively. This a value corresponds to the electron density of 7.2×10^{22} m^{-3}.

C. Translational Temperature and Electron Density Distribution

Based on the Voigt profile fitting method, the distribution of the translational temperature behind the shock front was determined as shown in Fig. 5, where the horizontal axis represents the distance measured from the shock front. The solid and the dashed lines are the translational and the vibrational temperatures predicted based on Park's two-temperature model, respectively. In the region just behind the shock front (less than 3 mm behind the shock front), it is not possible to determine the translational temperature because the absorption was not strong enough. This means that the oxygen atoms at the excited state are not sufficiently generated because

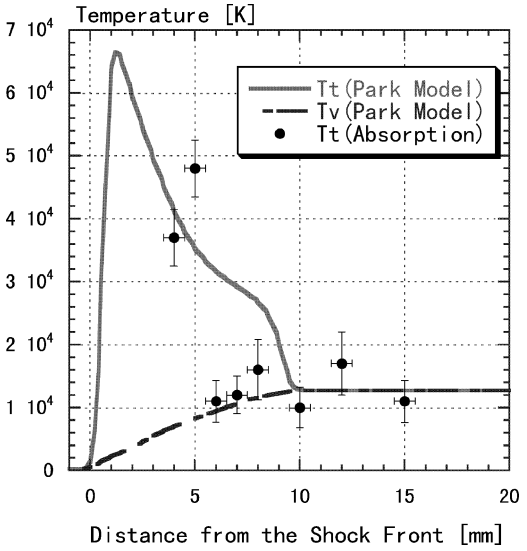

Fig. 5 Temperature distribution behind shock wave (shock propagation velocity 12.1 ± 0.1 km/s).

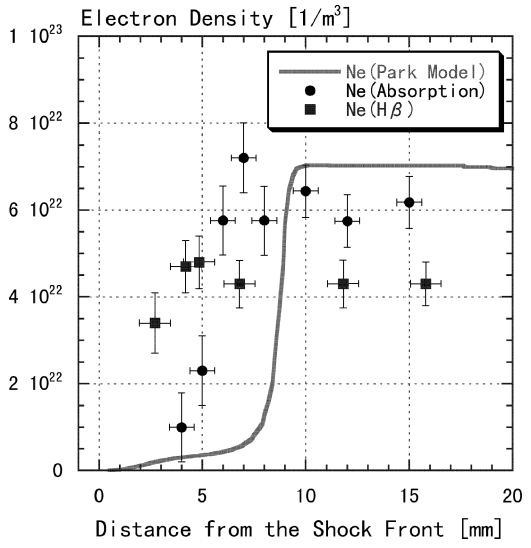

Fig. 6 Electron density distribution behind shock wave (shock propagation velocity 12.1 ± 0.1 km/s).

some incubation period is necessary for those atoms to be generated through the dissociation of molecular oxygen and the energy exchange process.

The translational temperature deduced from the experiment is approximately 4.0×10^4 K at around 5 mm behind the shock front. After that, it decreases sharply to a value of around 1.2×10^4 K and maintains an almost constant value afterward; that is, it reaches a plateau region. This tendency can be observed also in the theoretical prediction by Park's two-temperature model. That is, the translational temperature has a maximum value just behind the shock front and then quickly reaches a value equilibrated with the vibrational temperature. Therefore, the measured temperature at the plateau region is expected to correspond to the equilibrium value. The agreement with the prediction at the equilibrium region is reasonable.

As mentioned earlier, the collisional broadening in this experiment was mainly due to the Stark broadening. Therefore, by means of the Voigt profile fitting method, the electron density distribution was also determined. On the other hand, an experimental measurement of electron density in airflow by the use of the Stark effect of the Balmer beta (Hβ) line of hydrogen had been carried out previously.[6] Therefore, it is expected that the validity of the present result can be demonstrated by comparing these results for the electron density. Figure 6 shows the electron density distribution behind the shock wave. The filled circle represents the present result, whereas the filled rectangle and the solid line represent, for comparison, the result from the Hβ line of hydrogen and a numerical prediction by Park's two-temperature model, respectively. At a distance of 5 mm behind the shock front, the electron density determined from the absorption spectroscopy is slightly smaller than that determined previously. On the other hand, in the region more than 6 mm behind the shock front, the electron density determined from the absorption spectroscopy is slightly larger than the previous result. As seen in Fig. 6, the order of the electron density determined from the absorption spectroscopy agrees reasonably well with that determined previously. This agreement suggests that the present result based on the absorption spectral profile is fairly reasonable.

In Fig. 6, the discrepancy between the experimental results and the theoretical one is discernible up to 8 mm from the shock front. As already discussed in Refs. 3 and 6, this phenomenon was suggested to be caused by the photoionization at the region ahead of the shock wave, which is given rise to by the strong radiation just behind the shock wave.[14]

V. Discussion

Because, in the present experiment, two physical properties such as the translational temperature and electron number density were determined from the Voigt profile fitting, it is necessary to make a reasonable fitting not only in the central part of the spectrum, but in its wing part as well. With this aim, an appropriate weight is imposed especially for the wing part of the spectrum when the residual defined from the measured data and the Voigt profile was designed.

In the present deduction procedure, the uncertainties in the translational temperature and the electron density originated from the measurement error of the laser intensity. The error propagation from the laser intensity to the absorption coefficient [Eq. (1)] tells us that the estimated uncertainty of the absorption coefficient becomes from 6 to 10% at each wavelength of the absorption spectrum. These absorption coefficients uncertainties influence the uncertainty in the deduced values such as the translation temperature and the electron number density. In the present experiment, we estimate the uncertainty of at most 35% in the translational temperature and of at most 15% in the electron density. The reason for this rather large uncertainty was because of the rather large uncertainty in the absorption coefficient, which was given rise to because the logarithmic calculation is necessary to obtain the absorption coefficient from the measured laser intensity.

The present result clarified that translational temperature is almost comparable to the prediction based on the two-temperature model. On the other hand, the rotational temperature measured in Refs. 3 and 6 was much lower than the theoretically predicted translational temperature. Therefore, we can conclude that the rotational temperature measured previously is surely much lower than the translational temperature. Theoretically speaking, if the rotational temperature is lower than the translational temperature, the translational temperature may be larger than the prediction based on the two-temperature model. Unfortunately, because the uncertainty in the present translational temperature is relatively large, it is difficult to judge whether the measured translational temperature is larger than the theoretical one. On the other hand, another theoretical investigation of the rotational relaxation process in Ref. 15 suggested that the rotational temperature could not be as low as the experimental results in Refs. 3 and 6. To solve this discrepancy, we must continue further investigations both experimentally and theoretically. In relation to the experiment, however, we must remember the following: The rotational temperature in Refs. 3 and 6 was determined from the band spectrum of $N_2(2+)$, which is the transition from the $C_3\Pi_u$ state to the $B_3\Pi_g$ state, that is, higher excited states, and was assumed to be the equilibrium of the rotational temperature between the electrical states or the equilibrium between the ground state (X state) and the highly excited state (C state) of N_2. It is, however, still an open question whether this assumption is reasonable. To answer this question, the rotational temperature in the ground state should be investigated experimentally. However, this must remain for future work.

Based on the absorption spectrum, it may be possible to determine directly the number density of the atomic oxygen at the lower

state of the absorption transition (3s ^{5}S state) by integrating the spectrum profile. Unfortunately, because the 3s ^{5}S state is the metastable state, we cannot simply assume the Boltzmann relation between the ground state and the metastable 3s ^{5}S state. That is, to determine the number density in the ground state, we should know the possible distribution of the electronic excitation states. To accomplish this, a detailed analysis of the energy exchange process between the metastable state and other states must be carried out. For example, we must consider the deexcitation process from the metastable to the ground state, which is known to be mainly due to the quenching process caused by collisions between atomic oxygen at the metastable state and other particles. Unfortunately, it is expected that those processes are quite complex, and, therefore, they must must remain the subject of future work.

VI. Summary

To measure the translational temperature directly, which has not yet been carried out, the absorption spectroscopic technique with two wavelength lasers was applied to a shock-tube experiment where the shock wave propagates with a speed of 12.1 km/s through air of an initial pressure of 0.3 torr. The absorption spectrum thus measured behind the shock front was analyzed based on the theoretical Voigt profile. When a best fit of the Voigt profile was made to the measured absorption spectrum, the translational temperature and electron density were determined.

As for the translational temperature, it becomes 4.8×10^4 K at 5 mm behind the shock front and sharply decreases to the equilibrium value, or around 1.4×10^4 K in the region more than 6 mm from the shock front. This tendency of the translational temperature almost agrees with the numerical prediction based on the two-temperature model, at least qualitatively. Quantitatively speaking, however, we must factor in the relatively large uncertainty in the present translational temperature. Based on the present translational temperature measurement, we can confirm the phenomenon of the lower rotational temperature compared with the translational temperature, which was suggested previously in Refs. 3 and 6.

The electron density distribution shows reasonable agreement with the previous experimental result, which was determined based on the emission spectroscopy for the Balmer line of hydrogen. This agreement suggests that the present absorption spectroscopic technique established for the shock-tube experiment is fairly reasonable.

References

[1]Kawaguchi, J., Fujiwara, A., and Sawai, S., "Sample and Return Mission from Asteroid Nereus via Solar Electric Propulsion," *Acta Astronautica*, Vol. 38, No. 2, 1996, pp. 87–101.

[2]Ohtsu, H., Fujita, K., Suzuki, K., and Abe, T., "Radiative Heating Analysis Around the MUSES-C Reentry Capsule at Superorbital Speed," AIAA Paper 98-2447, June 1998.

[3]Fujita, K., Sato, S., Abe, T., and Ebinuma, Y., "Experimental Investigation of Air Radiation Behind a Strong Shock Wave," *Journal of Thermophysics and Heat Transfer*, Vol. 16, No. 1, 2002, pp. 72–82.

[4]Fujita, K., Sato, S., Abe, T., Ohtsu, H., and Ebinuma, Y., "Electron Density Measurements Behind Strong Shock Waves by H-β Profile Matching," *Journal of Thermophysics and Heat Transfer*, Vol. 17, No. 2, 2003, pp. 210–216.

[5]Matsuda, A., Fujita, K., Sato, S., and Abe, T., "Experimental Study for the Shock Layer Generated in a Super-Orbital Reentry Flight," *Proceedings of 23rd International Symposium for Shock Waves*, The Univ. of Texas at Arlington, Paper 1001, July 2001.

[6]Matsuda, A., Fujita, K., Sato, S., and Abe, T., "Nonequilibrium Phenomena Behind Strong Shock Waves Generated in Superorbital Reentry Flight," *Journal of Thermophysics and Heat Transfer*, Vol. 18, No. 3, 2004, pp. 342–348.

[7]Wiese, W. L., Fuhr, J. R., and Deters, T. M., *Journal of Physical and Chemical Reference Data*, Monograph No. 7, National Inst. of Standards and Technology, New York, 1996, p. 345.

[8]Moore, C. E., "Atomic Energy Levels I," National Bureau of Standards, Circular of the National Bureau of Standards 467, Washington, DC, June 1949.

[9]Wiese, W. L., "Plasma Diagnostic Techniques," *Pure and Applied Physics*, 21. Academic Press, New York, 1965, Chap. 6, pp. 265–317.

[10]Griem, H. R., *Plasma Spectroscopy*, McGraw–Hill, New York, 1964, pp. 91, 468.

[11]Baer, D. S., Chang, H. A., and Hanson, R. K., "Semiconductor Laser Absorption Diagnostics of Atomic Oxygen for Atmospheric-Pressure Plasmas" AIAA Paper 93-0822, Jan. 1993.

[12]Posener, D. W., "The Shape of Spectral Lines: Tables of The Voigt Profile," Australian Journal of Physics, Vol. 12, No. 2, 1959, pp. 184–196.

[13]Ogura, E., Funabiki, K., Sato, S., and Abe, T., "Free Piston Double Diaphragm Shock Tube," Inst. of Space and Astronautical Science, Rept. 96, Kanagawa, Japan, Sept. 1997 (in Japanese).

[14]Fujita, K., Matsuda, A., Sato, S., and Abe, T., "Electron Temperature and Density Measurement ahead of Strong Shock Waves," AIAA Paper 2001-2765, June 2001.

[15]Fujita, K., and Abe, T., "State-to-State Nonequilibrium Rotational Kinetics of Nitrogen Behind Strong Shock Waves," AIAA Paper 2002-3217, June 2002.